Investigation of propeller effects on the Aurora aircraft

Zhang, F.; Khalid, M.; Syms, G. F.; Ball, N.

Publisher's version / Version de l'éditeur:
https://doi.org/10.2514/6.2001-2413
19th AIAA Applied Aerodynamics Conference, 2001-06-11

Numerical Investigation of Propeller Effects on the Aurora Aircraft

F. Zhang*, M. Khalid†, J. Syms‡ and N. Ball§
Aerodynamics Laboratory
Institute For Aerospace Research (IAR)
National Research Council of Canada (NRC)
Ottawa, Ontario, Canada K1A 0R6
Steve.Zhang@nrc.ca

Abstract[1]

The paper contains a numerical investigation into the effects of propellers on the flows around the Aurora CP-140 aircraft. The problem is approached by comparing the CFD results for both propeller-on and propeller-off configurations against the available experimental data. The structured multi-block compressible flow solver NPARC with Baldwin-Barth turbulence model was used for this investigation. Isolated propellers are modeled by the blade element theory with swirl and the flow conditions on these propeller disks are imposed at the appropriate locations for the full aircraft. Comparisons of pressure distributions are carried out for two angles of attack (low and moderate) at a freestream Mach number of 0.564.

Background

Two years ago, the Institute for Aerospace Research, National Research Council of Canada (IAR, NRC) was asked by Department of National Defense of Canada (DND) to investigate the aerodynamic performance of the Aurora maritime patrol aircraft (designate CP-140). This study was part of a larger project aimed at extending the useful life of this aircraft in Canadian Forces as well as other military fleets around the world. The investigation involved both experimental and CFD studies. The CFD analyses sought out information on several issues including the side-wall boundary layer effects [1], the sting interference problems [2] on the models installed in the IAR wind tunnels, the flow field around the complete 3D configuration [3] and the modeling of the propeller flow around the complete aircraft. This paper concentrates on the numerical calculations for the Aurora aircraft with and without propeller configurations. Through comparing the computed results for these two configurations, the effects of the propellers on the flow around the aircraft are addressed.

Introduction

The analysis of the flow generated by a propeller is important in the design phase of a propeller-driven aircraft. In the slipstream behind the propellers, the flow properties are significantly different from the properties in the freestream. Surfaces of the configuration inside the slipstream experience other forces with the propellers-on than they do in freestream flow. As in reality, all of the propellers of this aircraft were modeled to rotate in the same direction. This will give rise to asymmetric forces and moments on the aircraft which may have important implications upon aerodynamic performance. Nowadays, the successful integration of propulsion systems on modern aircraft becomes a very challenging work and an important feature in the design and development of advanced technology aircraft. This challenge can only be tackled by combining experiments in high quality aerodynamic test facilities and high-level CFD simulations.

This paper focuses on the numerical simulations of the flowfield over Aurora aircraft with propellers-off (Config. 1) and propellers-on (Config. 2) configurations. To incorporate the effects of the propellers on the full aircraft, the propellers are first modeled by the blade element theory. The total pressure jump and the swirl velocity across the disks are applied. A radial

* Assistant Research Officer
† Group Head, Member AIAA
‡ Research Officer
§ Project Manager

distribution based on a sixth order Bessel function generates a realistic load distribution on each propeller. The flow conditions existing at the isolated disks are then imposed on the disks of the full aircraft. This model of the propeller, in which the jump conditions at the disk are uncoupled from the flow around the aircraft, provides an initial low-order approximation to the fully-coupled installed propeller. The effects of the propellers on the flowfield can be seen clearly through comparing the CFD results between these two configurations. .

Description of the Grid Generation

The structured computational grid used in this CFD study is generated interactively on a Silicon Graphics workstation using ICEMCFD Hexa [4], which is a 3D object-based, semi-automatic, multi-block surface and volume mesher.

It is found that the most involved and labor intensive aspect of this exercise is the preparation of the structured grid around such complex geometry as the Aurora aircraft. The problem becomes even more challenging when dealing with grids intended to resolve viscous flows. For the complete aircraft with both propeller-on and propeller-off configurations, the comparison of the computed flowfield under two configurations would provide a good assessment of the effects of the propeller wake as it impinges upon wing and other surfaces of the aircraft. Under normal operating conditions, all the propellers rotate in the same counter clockwise mode. This produces an obvious asymmetry in the flow field. The computation for the complete aircraft configuration must be simulated. Considering this situation, the grid generation for the above two configurations utilizes the same topology. The grid generation for the entire aircraft configuration with propellers is treated as the primary mesh. When deriving the grid for the propellers-off configuration, the blocks representing the propeller are declared as flow-through blocks, otherwise, they are assigned by the appropriate wall or disks boundary conditions to identify their actual functions.

Figure 1 displays the aircraft surfaces for the computational propellers-on and propellers-off configurations, respectively. For the Aurora without propellers, the grid contains 253 blocks and 9.22 million nodes. And for aircraft with propellers, the grid contains 237 blocks and 9.19 million nodes.

Computations and Discussions

The computations are carried out using NPARC solver package supplied by AEDC/NASA [5,6]. Two algorithms, the Beam-Warming algorithm and the multi-stage Runge-Kutta algorithm, are available in the package. The Beam-Warming algorithm is selected for the present computations. This is an implicit, computationally robust scheme for solving the Navier-Stokes equations. In order to suppress the numerical oscillations and odd-even point de-coupling, the Jameson-style artificial dissipation is used. A number of turbulence models are available in the package. Based on the past experience with this package for computing flows under current freestream condition, the Baldwin-Barth one-equation model is selected.

The computation is carried out for two flow cases, which are typical of the flow conditions used in the experiment,

(1) $M_\infty = 0.564$, $\alpha = 0.0$ and $Re/m = 1.41\times10^7$
(2) $M_\infty = 0.564$, $\alpha = 3.9$ and $Re/m = 1.41\times10^7$

Solution convergence was determined by monitoring the history of the residuals. In all cases, the residuals were reduced by about 3 orders of magnitude to ensure a converged solution. At least 8000 iterations were required for a satisfactory convergence.

For the calculations on the Aurora aircraft with propellers-on configuration, the thrust coefficient and the advance ratio were set at 0.1827 and 3.13 respectively.

The results obtained from computations on Configuration 1 and 2 are shown in Figure 2. The pressure coefficient distributions on the upper surfaces of the two configurations are shown in Figure 2(a) and Figure 2(b). Figure 2(c) and Figure 2(d) display the pressure coefficient distributions on the lower surfaces. Figure 3(a) and Figure 3(b) refer to the resultant flow field difference between propellers-off and propellers-on configurations, for upper and lower surfaces respectively. Due to the unidirectional rotating propellers, the flowfiled is no longer symmetric. This phenomenon is demonstrated from these figures.

The asymmetric nature of the flow can also be deduced from the pressure plots on the left wing

and horizontal tail planes in contrast to the counterparts on the right side. Figure 4 shows the actual spanwise stations where the pressure coefficients at the right and left wings and horizontal tail planes were extracted. For both propellers-on and propellers-off configurations, the pressure comparisons between the computations and the experiments in the wing region are shown in Figure 5(a) to 5(e). It should be noticed that the experimental data shown in the plots refers to the half-model configurations (right side) and the calculations are carried out for the complete models. It is apparent from these figures that there is a significant effect due to the presence of the propellers, which shows up as the differences in pressure coefficient between the left and right wings. The trends between the various data are consistent with measurements. The comparison between the absolute values is not as spectacular. With the exception of the most inboard solution, the computed data seems to pick up the suction peak well. The agreement near the trailing edge between the computations and the measurements is not as good mostly due to the grid degeneration effects in this region. The same comparison of the pressure data on the horizontal tailplane as observed in Figure 5(f) and 5(g) shows good agreement between the computed and measured values. It is also noted from these figures that the differences of the experimental data between propellers-on and propellers-off configurations are small. This is expected for the low thrust coefficient propeller-driven flows.

For the flow conditions in Case 2, the pressure fields on the upper surface for both two configurations are shown in Figure 6(a) to 6(b). The pressure fields on the lower surface for the same two configurations are contained in Figure 6(c) to 6(d). The resultant differences in pressure fields between the two configurations under this case are shown in Figure 7(a) and 7(b) for the upper and lower surfaces respectively. Asymmetry in the flow is well demonstrated by the high pressure difference on the left wing-fuselage junction and the flow on the outboard wing regions.

The pressure plots at the five spanwise wing locations for the two configurations are shown in Figure 8(a) to 8(e). The experimental data shown here is once again relevant to the half-model configuration. It is very encouraging to note that except for the leading edge region, the agreement between the experiment and the computed results is quite reasonable. The horizontal tailplane comparison for this case is shown in Figure 8(f) and 8(g) at the two spanwise locations respectively. The difference in pressures between the propellers-on and propellers-off configurations turned out to be small as the tailplane is situated at some distance from the wing.

Conclusions

CFD provides a reliable method of obtaining detailed flow field information past complex aircraft configuration. It offers a good insight for designing comprehensive wind tunnel test schedules.

The unidirectional rotation of the propellers leads to flow asymmetries which are well demonstrated by the computation. The computed data provided satisfactory comparisons against the measured data. For accurate assessments of the propeller's effects in measurements, the complete model test would be most appropriate.

Acknowledgment

This work was carried out in collaboration with the Canadian Department of National Defense (DND). The authors would like to thank NPARC Alliance for permitting the use of NPARC for this work.

References

1. F. Zhang, M. Khalid, H. Xu and N. Ball, "Numerical Prediction of the Reflection Plate Boundary Layer Effects on Half Model in Wind Tunnel," AIAA-2000-2376, Jun. 2000, Denver, USA.
2. Kumar, S., "CFD Study of Sting Effect – Stage 1," Technical Report in IAR, Sep. 1999.
3. J. Su and J.T. Conway, "Numerical Analysis of the Aerodynamics of the Aurora Aircraft by an Inviscid/Viscous Interaction Method," 22nd International Congress of Aeronautical Sciences, Aug. 2000, Harrogate, UK.
4. http://flash.icemcfd.com/index.html
5. NPARC User's Guide- NASA LeRC/AEDC Alliance, Version 3.0, Sep. 1996. Washington.
6. Cooper, G. K. and Sirbaugh, J. R., "Parc Code: Theory and Usage," AEDC-TR-89-15, Sverdrup Technolgy Inc.

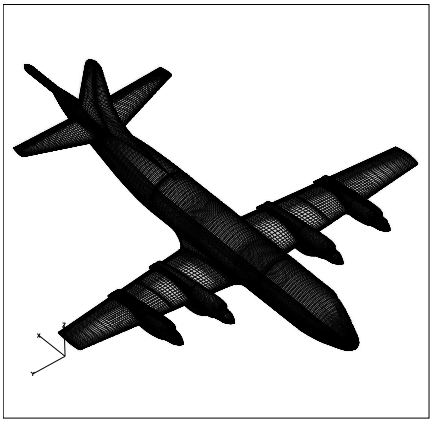

Figure 1(a)

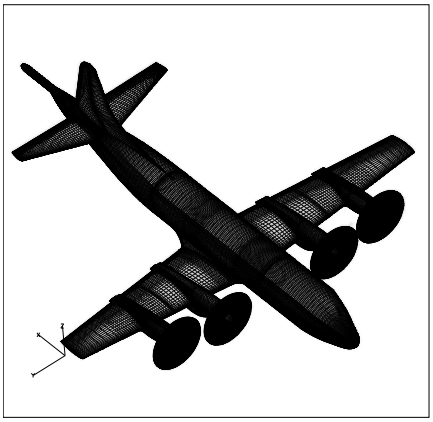

Figure 1(b)

Figure 1. The Geometry and Mesh on Aurora Aircraft Surfaces

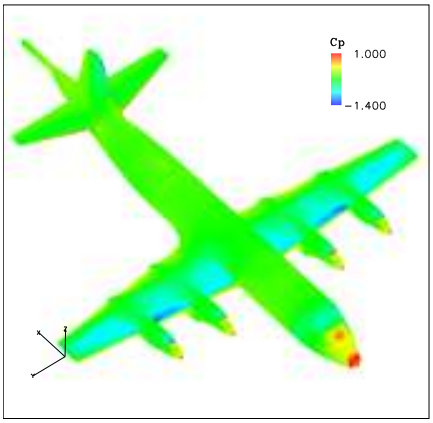

Figure 2(a)

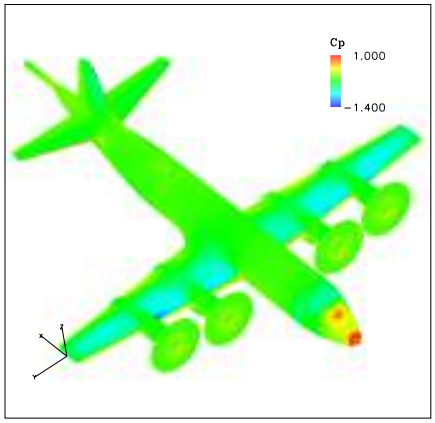

Figure 2(b)

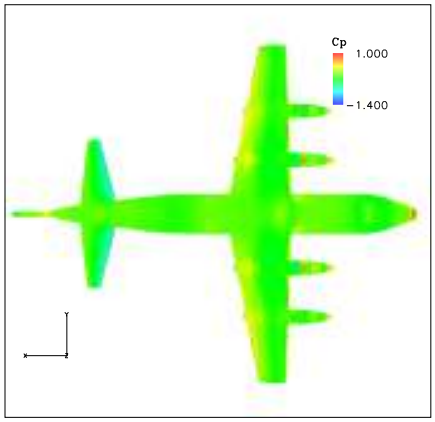

Figure 2(c)

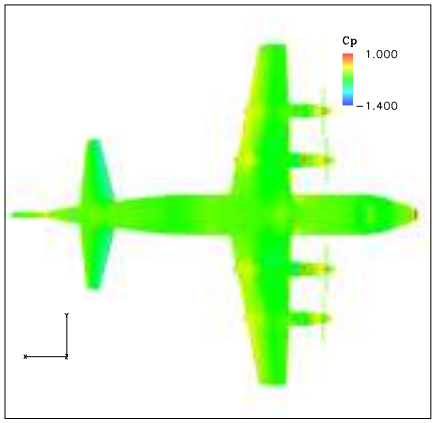

Figure 2(d)

Figure 2. Pressure Coefficient Distributions On Aurora Aircraft, $M_\infty = 0.564$, $\alpha = 0.0$

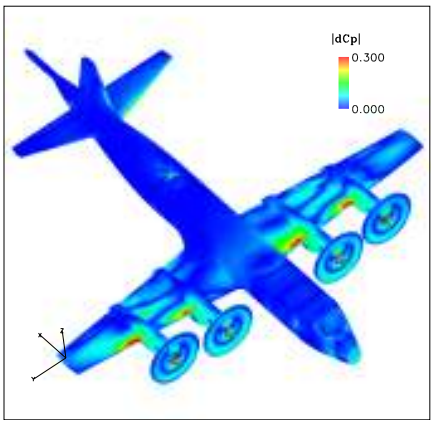

Figure 3(a)

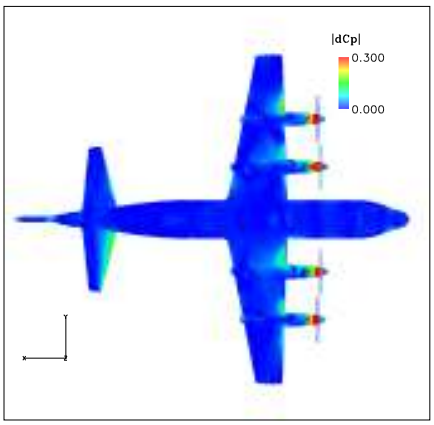

Figure 3(b)

Figure 3. Pressure Coefficient Differences Between Two Configurations, $M_\infty = 0.564$, $\alpha = 0.0$

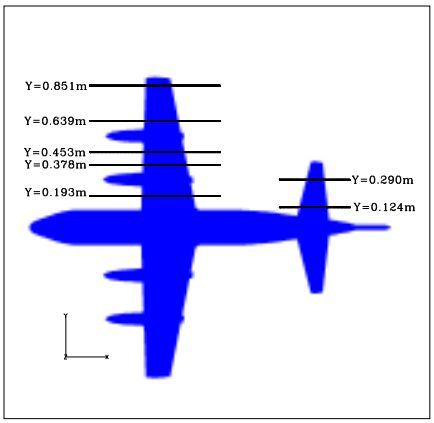

Figure 4. Five Wing Span-Wise and Two Horizontal Tail Span-Wise Locations

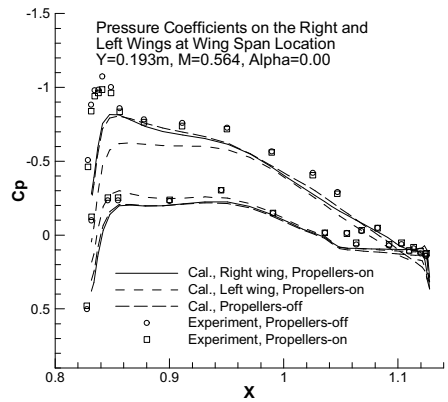

Figure 5(a)

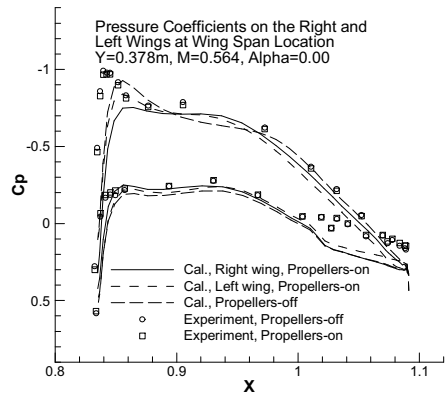

Figure 5(b)

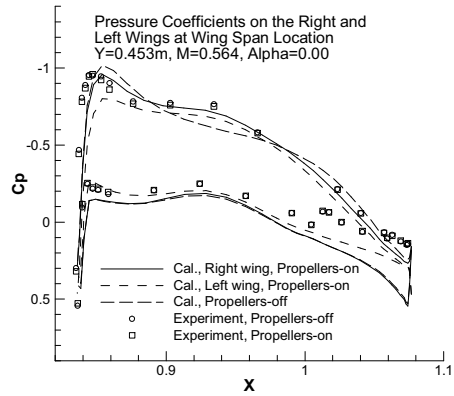

Figure 5(c)

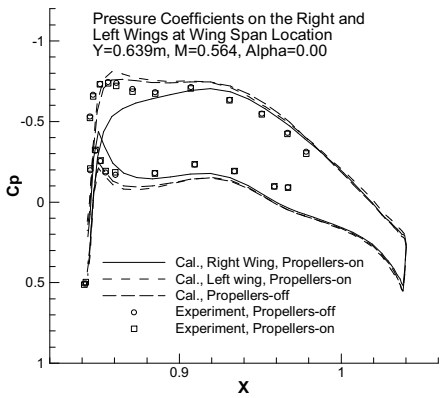

Figure 5(d)

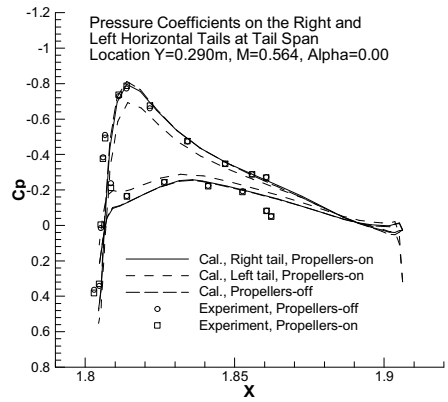

Figure 5(g)

Figure 5. Pressure Coefficient Plots on the Wings and Horizontal Tails, $M_\infty = 0.564$, $\alpha = 0.0$

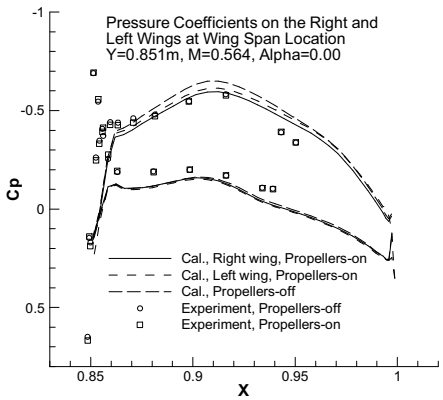

Figure 5(e)

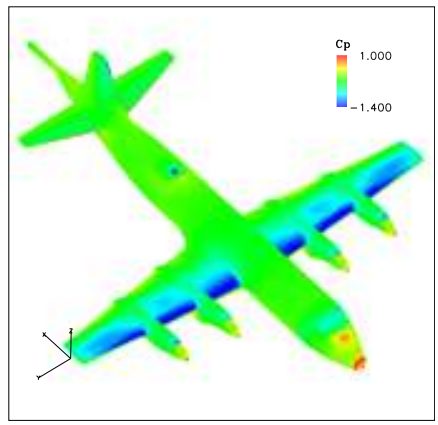

Figure 6(a)

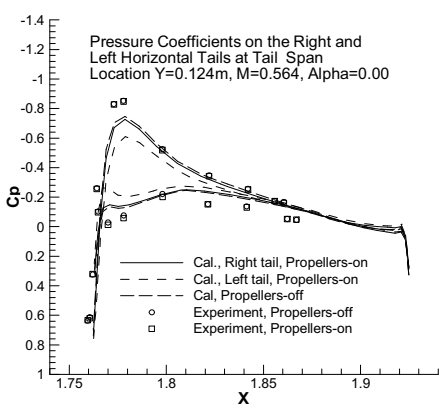

Figure 5(f)

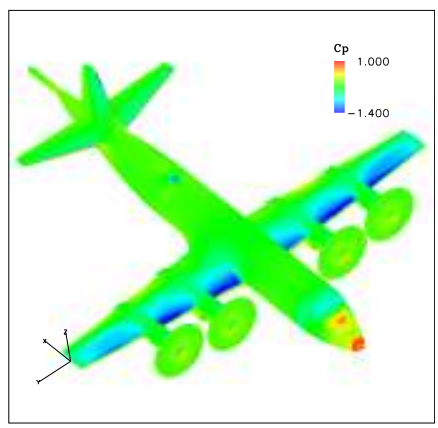

Figure 6(b)

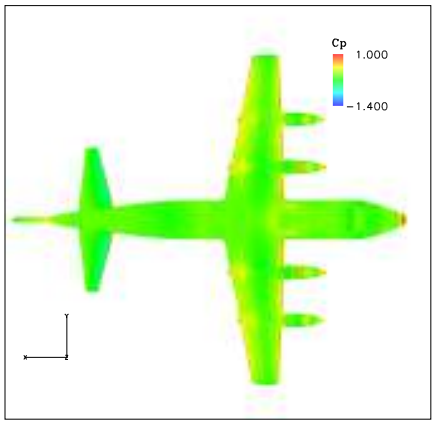

Figure 6(c)

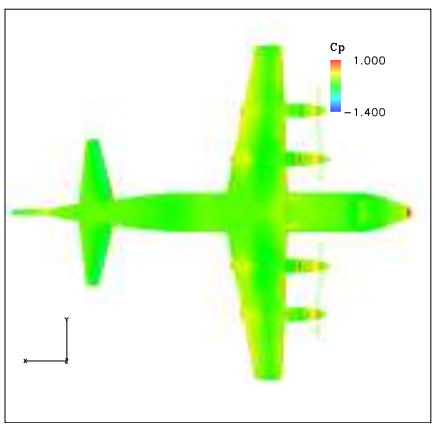

Figure 6(d)

Figure 6. Pressure Coefficient Distributions On Aurora Aircraft, $M_\infty = 0.564$, $\alpha = 3.90$

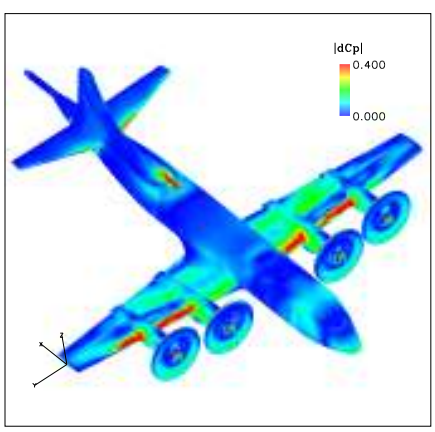

Figure 7(a)

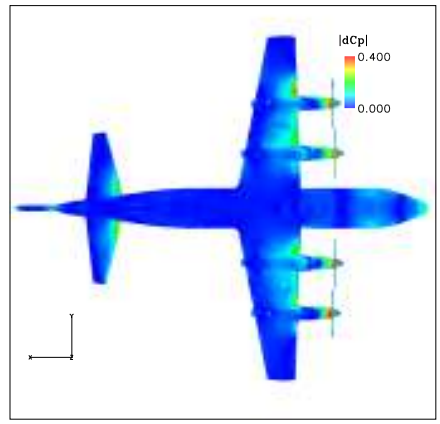

Figure 7(b)

Figure 7. Pressure Coefficient Differences Between Two Configurations, $M_\infty = 0.564$, $\alpha = 3.90$

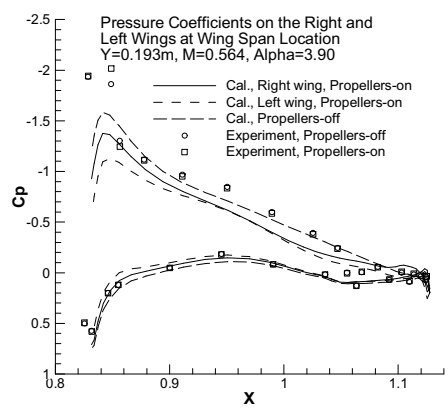

Figure 8(a)

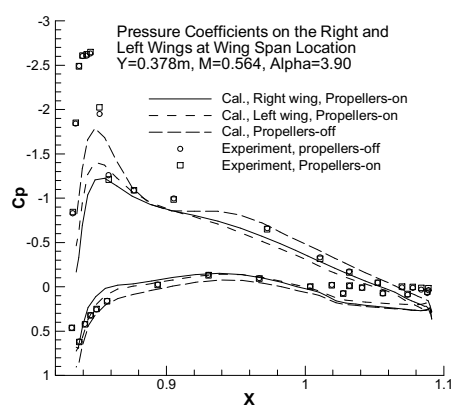

Figure 8(b)

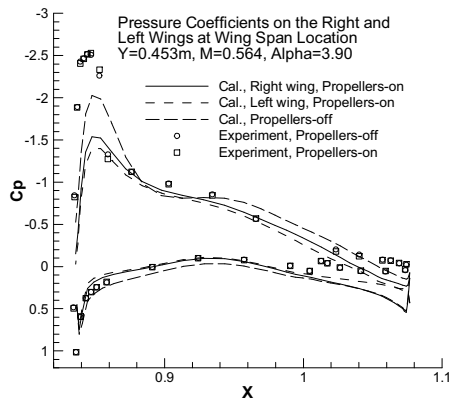

Figure 8(c)

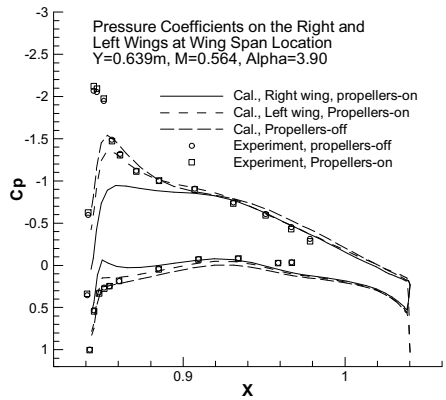

Figure 8(d)

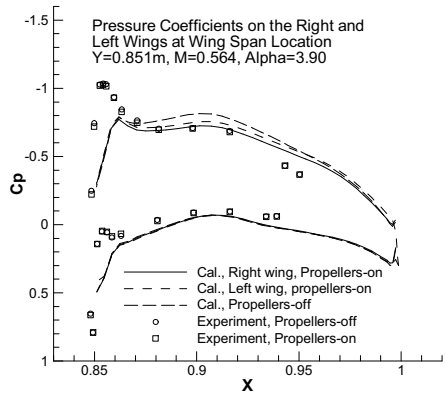

Figure 8(e)

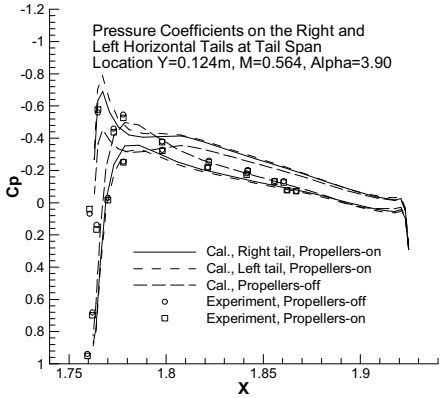

Figure 8(f)

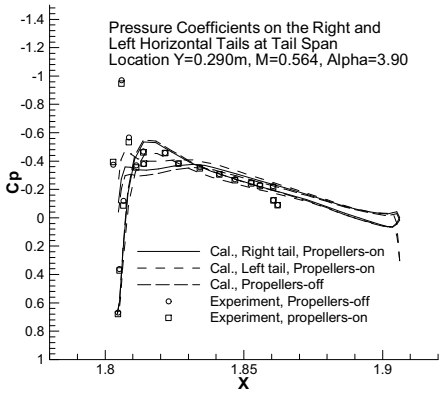

Figure 8(g)

Figure 8. Pressure Coefficient Plots on the Wings and Horizontal Tails, $M_\infty = 0.564$, $\alpha = 3.90$